International Journal of Ocean System Engineering 3(2) (2013) 77-89
http://dx.doi.org/10.5574/IJOSE.2012.3.2.077

On Propeller Performance of DTC Post-Panamax Container Ship

Omer Kemal Kinaci[1*], Abdi Kukner[2] and Sakir Bal[3]

[1]*Faculty of Naval Architecture and Maritime, Yildiz Technical University, Istanbul, 34349, Turkey*

[2]*Faculty of Naval Architecture and Ocean Engineering, Istanbul Technical University, Istanbul, 34469, Turkey*

(Manuscript Received March 15 2012; Revised April 10, 2012; Accepted May 3, 2012)

Abstract

The propeller performance has been investigated using a benchmark Duisburg Test Case ship with RANSE. First, the hydrodynamic characteristics of propeller in case of open water have been analyzed by a commercial CFD program and the results are compared with those of experimental data. Later, the flow around the bare hull has been solved and the frictional resistance value and form factor of the ship have been obtained and compared with those of ITTC57 formulation and experimental results for validation. The free surface effect has been ignored. A good agreement has been obtained between the results of RANSE and experiments at both stages. Then the ship - propeller interaction problem was solved by RANSE and the differences in thrust, torque and efficiency of propeller as compared with the open–water numerical results have been discussed.

Keywords: Ship – propeller interaction, Propeller performance, RANSE, CFD, Self – propulsion point

1. Introduction

With the aid of enormously growing computer technology, Computational Fluid Dynamics (CFD) solutions on ship resistance and propulsion have increased rapidly in recent years. One can have a general idea of this reality by counting the number of CFD based papers published in journals and conference proceedings and due to this fact research has been switched to advanced subjects and more complex geometries. Constitution of an experimental setup is an expensive alternative and although experiments can give some part of solutions of the flow field, CFD provides with comprehensive information [1].

Computer technology has made a breakthrough during 1980s, becoming cheaper and faster every day. Up to that date, potential methods were forming the core of the analyses excluding the effects of viscosity and turbulence. The analyses covered one part of the ship generally; which would be the bare hull, propeller or the rudder only. However; computers have allowed more complex analyses and the attention then started to evolve to the interactions of the appendages with the ship hull. Propeller – hull interaction had drawn attention in these times. For example, analyzing the history of the Symposium on Naval Hydrodynamics, propeller hull interaction was seen to be a major subject first in 1984 when the 15th of the series of the symposium was held. A previous symposium held just in 1980 has no articles based on the interaction concept while in the 15th symposium propeller – hull interaction covered two sessions. In that symposium, a total of eight papers were presented in two sessions with many of them being experimental works. These experimental works have paved the way for numerical studies but some numerical studies have also been made at that time and one of them was a paper published by Zhou and Yuan. Their study covered two- equation $k-\varepsilon$ turbulence model to solve the flow near the stern,

*Corresponding author. Tel.: +90-212-3833015, Fax.: +90-212-3833021
E-mail address: kinaci@yildiz.edu.tr

and the propeller was modeled by using a lifting line theory [2]. The thrust deduction and the effective wake of the system were accurately calculated with their method.

There are more experimental works on the subject than numerical works due to the complex system of the rotating flow induced by the propeller. But besides that, the emergence of some commercial and professional CFD codes has allowed many scientists to gain insight about the propeller hull system. Some recent numerical works are summarized here. For instance, Shen et al. have investigated the hydrodynamic performance of a ship with a propeller numerically. They have used RANSE with CFD and validated their solutions with the existing experimental data [3]. Tocu and Lungu predicted the hydrodynamic performance of a ship hull with a propeller [4]. The free surface effects are included in their study. Stück et al. redesigned a ship hull and optimized the wake in the light of propeller-ship interaction [5]. Lee and Chen have looked at the ship-propeller interaction from the cavitation point of view and have investigated the interaction effect on propeller induced cavitating pressure [6]. Szelangiewicz and Abramowski have worked on the hull form modification on ship resistance and propulsion characteristics [7, 8, 9]. A part of their work was to calculate the effects of the ship hull on the hydrodynamic characteristics of the propeller. Not only the propeller-hull system but also propeller-rudder-hull system was also analyzed using commercial CFD codes. Lungu and Pacuraru have solved the flow problem around a container ship that has rudder and propeller with finite volume method using RANSE [10].

The effect of propeller swirl was taken into account and effective wake was also calculated. The flow around a ship with all its appendages were investigated by Muscari and his colleagues both experimentally and numerically [11]. Experimental works were carried out by LDV while numerical studies were done with a commercial software using RANSE.

There are many experimental studies about the ship hull interaction with its appendages; some of these are listed here. A work made by Felli and Felice investigates the wake of a propeller by LDV experimentally [12]. They have aimed to pave the way for numerical studies that may be developed in the future. Again an experimental work by Felli and his colleagues' focused on the propeller and rudder without a ship hull form [13]. The work emphasized on the low performance of rudder working behind the propeller producing corrupted flow. Carlton et al. have worked on the interaction of the appendages with the ship hull based on CFD, model tests and sea trials [14]. The interaction was examined for rudder design. In that work, rudder's contribution to the overall propulsion efficiency for different designs was tested.

2. Hydrostatic Properties of the Ship and The Propeller

In this study, a benchmark post-panamax container ship called Duisburg Test Case (in short notation, DTC) has been used [15]. The hull and propeller geometries have been spread online. The results of open water propeller tests, resistance tests and propulsion tests are also accessible.

Main particulars of the model and the full ship are given in table 1.

Table 1. Main dimensions of DTC

	(units)	Model Scale	Full Scale
L_{pp}	(m)	5.976	355
B_{wl}	(m)	0.859	51
T_m	(m)	0.244	14.5
V	(m^3)	0.827	173467
C_B	-	0.661	0.661
S_w	(m^2)	6.243	22032

Table 2. Propeller parameters of DTC

	(units)	Model Scale	Full Scale
D_P	(m)	0.15	8.911
$P_{0.7}$ / D_P	-	0.959	0.959
A_e / A_0	-	0.8	0.8
$c_{0.7}$	(mm)	0.054	3.208
θ_{eff}	(^{o})	31.97	31.97
d_h / D_p	-	0.176	0.176

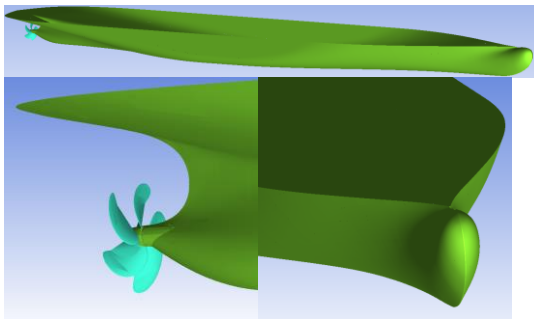

Fig. 1a (above). A perspective view of hull form of DTC. Figure 1b (left, below). The stern form with the propeller. Figure 1c (right, below). The bow form with the bulb.

The model to full ship scale ratio is 1 / 59.407. The propeller parameters of Duisburg Test Case are given in table 2. Again, the model to full scale ratio is 1 / 59.407.

The underwater hull form of Duisburg Test Case is given in figure 1a. A close up view of the stern and the bow forms can also be seen from figures 1b and 1c, respectively. The figures only show the underwater hull form. More details about the ship and the propeller can be found in reference [15]. The experimental data is also available in the same article.

3. Method

In this study it is analyzed the effect of the ship hull on the propeller efficiency with a commercial RANSE solver. The momentum equation of the flow, also known as the Navier – Stokes equation, can be written as;

$$\rho\frac{Dui}{Dt} = Fi - \frac{\partial p}{\partial xe} + \mu\nabla^2 ui \qquad (1)$$

This equation usually holds for laminar flows, however; ships work on high Reynolds numbers. Due to this reason, the flow around the hull (especially at the stern) is highly turbulent. Originating from the complex behavior of turbulence and their unpredictable effects on the flow, time averaged values of parameters are brought into the equation. The relation between the flow velocities, average values of parameters and oscillations in time can be defined as:

$$u = \bar{u} + u' \quad v = \bar{v} + v' \quad w = \bar{w} + w' \qquad (2)$$

Here, u, v, w are components of flow velocities of a point in the directions of x, y and z respectively, and u', v', w' are oscillations in flow velocities at that same point. This approach is called RANSE (Reynolds Averaged Navier Stokes Equation) and the time averaged equations of Navier – Stokes and continuity give rise to an equation in tensoral notation:

$$\rho\frac{D\overline{u_i}}{Dt} = F_i - \frac{\partial \bar{p}}{\partial x_i} + \mu\nabla^2\overline{u_i} - \rho\left(\frac{\partial\overline{u'_i u'_j}}{\partial x_i}\right) \qquad (3)$$

Here $\bar{u_i}, \bar{p}$ ve $\overline{u_i u_j}$ define the average values of parameters in time.

The last term in the RANSE equation (equation (3)) is the Reynolds stress component and refers to the oscillations in time. By considering equation 2, the continuity equation can be defined as:

$$\frac{\partial\rho}{\partial t} + \frac{\partial\rho\bar{u}}{\partial x} + \frac{\partial\rho\bar{v}}{\partial y} + \frac{\partial\rho\bar{w}}{\partial z} = 0 \qquad (4)$$

Again, the time averaged values of parameters in time are used in the continuity equation. In this study, the flow is accepted to be steady and incompressible and the effects of free surface and cavitation are ignored. Due to the incompressible flow, the energy equation is automatically eliminated from the conservation equations and only the continuity and momentum equations would be left. After several simplifications, the conservation equations will be in the form;

$$\frac{\partial\bar{u}}{\partial x} + \frac{\partial\bar{v}}{\partial y} + \frac{\partial\bar{w}}{\partial z} = 0 \qquad 5(a)$$

$$\rho\left(\bar{u}\frac{\partial\bar{u}}{\partial x} + \bar{v}\frac{\partial\bar{u}}{\partial y} + \bar{w}\frac{\partial\bar{u}}{\partial z}\right) = -\frac{\partial\bar{p}}{\partial x} + \mu\nabla^2\bar{u} - \rho\left(\frac{\partial\overline{u'u'}}{\partial x} + \frac{\partial\overline{u'v'}}{\partial y} + \frac{\partial\overline{u'w'}}{\partial z}\right) \qquad 5(b)$$

$$\rho\left(\bar{u}\frac{\partial\bar{v}}{\partial x} + \bar{v}\frac{\partial\bar{v}}{\partial y} + \bar{w}\frac{\partial\bar{v}}{\partial z}\right) = -\frac{\partial\bar{p}}{\partial y} + \mu\nabla^2\bar{v} - \rho\left(\frac{\partial\overline{v'u'}}{\partial x} + \frac{\partial\overline{v'v'}}{\partial y} + \frac{\partial\overline{v'w'}}{\partial z}\right) \qquad 5(c)$$

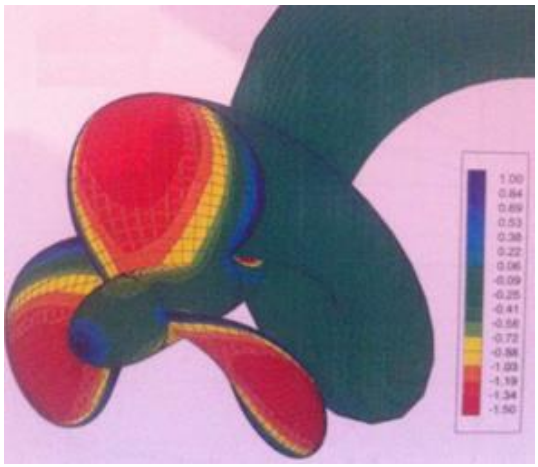

Figure 2a. Pressure coefficient distribution of DTMB4119 by Brandner [17].

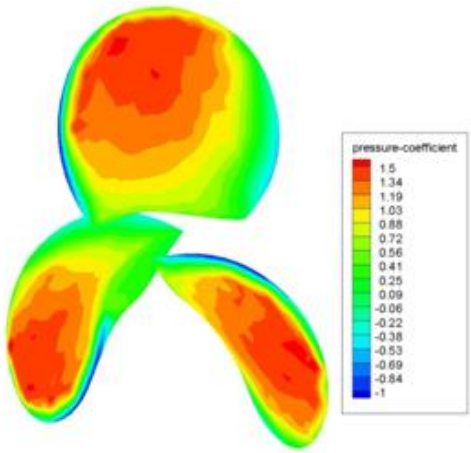

Figure 2b. Pressure coefficient distribution of DTMB4119 found in this study.

$$\rho(\bar{u}\frac{\partial \bar{w}}{\partial x}+\bar{v}\frac{\partial \bar{w}}{\partial y}+\bar{w}\frac{\partial \bar{w}}{\partial z}) = -\frac{\partial \bar{p}}{\partial z}+\mu\nabla^2\bar{w}-\rho(\frac{\partial \overline{w'u'}}{\partial x}+\frac{\partial \overline{w'u'}}{\partial y}+\frac{\partial \overline{w'w'}}{\partial z}) \quad 5(d)$$

These four equations in equation set (5) make up the brick of RANSE used in this study. Here there are seven unknown parameters; $\bar{u},\bar{v},\bar{w},\bar{p},u',v',w'$. Linking the equations obtained from turbulence models and boundary conditions to the conservation equations, the problem becomes mathematically solvable. For a broader explanation of the theory of RANSE and its numerical implementation, refer to [16]. Details of the used turbulence model are given in the next section.

4. CFD validation with open water propeller test results

At the first step, a tested propeller DTMB4119 was solved with CFD to validate the results. DTMB4119 has a wide range of study both numerically and experimentally; therefore, it is used as a guide before solving for DTC propeller.

The details used in the CFD program will not be explained extensively here, since they have already been mentioned in detail in the following section. All factors selected for the solution of this propeller has been also used for the DTC propeller. The predicted pressure coefficient for DTMB4119 is compared with the results of Brandner [17]. The comparison is given in figure 2. In Figure 2b the negative pressure coefficients have been shown to be attuned to the color scheme of figure 2a.

Table 3a. Propeller performance of DTMB4119 found in three different ways.

	CFD			LIFTING SURFACE			EXPERIMENT		
J	K_t	K_q	η	K_t	K_q	H	K_t	K_q	H
0.5	0.276	0.0455	0.4831	0.2606	0.0456	0.4546	0.285	0.0477	0.489
0.6	0.2396	0.0405	0.5651	0.2305	0.0418	0.5264	-	-	-
0.7	0.2011	0.0351	0.638	0.1969	0.038	0.5771	0.2	0.036	0.632
0.8	0.1615	0.0296	0.6952	0.1634	0.0304	0.684	-	-	-
0.833	0.1488	0.0278	0.7099	-	-	-	0.146	0.028	0.692
0.9	0.1223	0.024	0.73	0.1262	0.0266	0.6794	0.12	0.0239	0.725
1	0.0809	0.0179	0.7182	0.0868	0.019	0.7269	-	-	-
1.1	0.0379	0.0114	0.583	0.0452	0.0152	0.5203	0.034	0.0106	0.575

Table 3b. Error percentages of open water propeller coefficients compared to the experiment.

	CFD			LIFTING SURFACE		
J	K_t	K_q	H	K_t	K_q	η
0.5	3.1579	4.6122	1.2065	8.5614	4.4025	7.0348
0.7	0.5470	2.5000	0.9404	1.5500	5.2632	8.6867
0.9	1.8806	0.4167	0.6849	4.9128	10.1504	6.2897
1.1	10.2902	7.0175	1.3722	24.7788	30.2632	9.5130

The results for propeller performance found in this work for DTMB4119 are better than those in the potential methods. The CFD results are closer to the experimental ones than those of produced by the potential methods. The digital performance values of DTMB4119 propeller found with three different ways are given in table 3a. The lifting surface and the experimental results are derived from Bal's work [18]. The error percentages of both methods compared with the experimental values where available are given in table 3b.

The error in table 3b is calculated as;

$$Error = \left| \frac{(CFD\ or\ Lifting\ Surface) - Experiment}{\max(CFD\ or\ Lifting\ Surface, Experiment)} \right|$$

As it can be seen from table 3a and table 3b, CFD produces more compatible results with the experiments. The same solution procedure is applied to the DTC propeller and the factors used before running the program are explained below.

The flow around the propeller in open water is solved with 1 million tetrahedral meshes. The water density is 998.47kg/m^3 and the water kinematic viscosity is 1.044*10^{-6}m^2/s for convenience with reference [15].

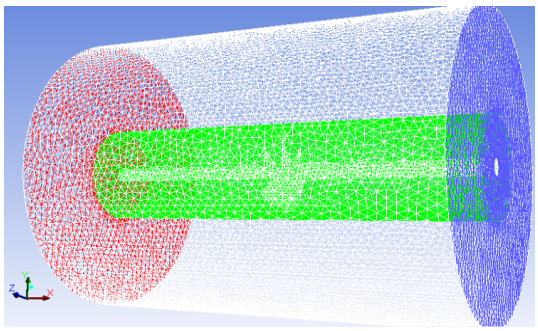

Figure 3. A perspective view of the open water propeller domain.

The realizable $k-\varepsilon$ turbulence model with standard wall function is used and the effects of cavitation are ignored. The propeller is thought to be deeply submerged in water: no free surface effects are included. The fluid domain is divided into two parts: inner part rotates with the propeller while the outer part has no rotation. Please refer to figure 3 for a view of the domain.

The rotation of the inner domain is equal to the number of revolutions that the propeller makes in a minute. The inlet velocity is held to be constant in the analyses and the number of revolutions of the propeller is constantly changed to have different advance coefficients J. The inlet velocity in the analysis is set to be 1.335m/s.

The wall boundary condition is specified at the boundary of the outer wall. The propeller blades are rotating relative to the adjacent cell zone, which is in the inner fluid domain. The turbulent intensity is 1% and turbulent viscosity ratio is 1. The least square cell based SIMPLE scheme for pressure-velocity coupling is used. The pressure, momentum, turbulent kinetic energy and turbulent dissipation rate are all in second order. The under relaxation factors are set to have default values. The solutions converge after about 1,000 iterations.

The comparison of CFD results with those of

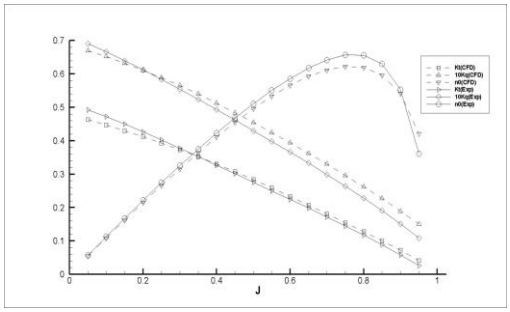

Figure 4. Comparison of CFD and experiment for propeller performance

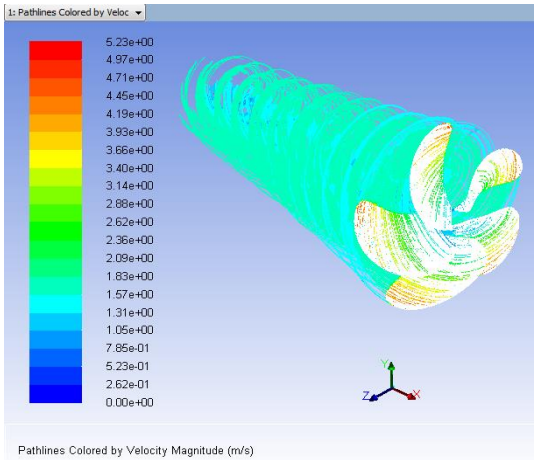

Fig. 5. Propeller swirl at J = 0.8

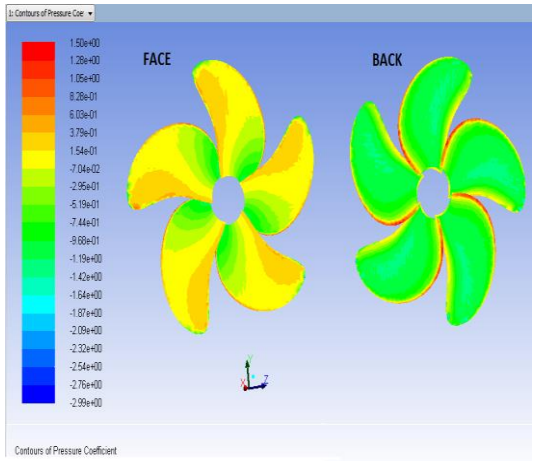

Figure 6. Pressure coefficient contours on the propeller

experiments can be seen in figure 4. A tabulated form of the results is also given in table 4.

The propeller swirl can be seen by plotting the path-lines released from the propeller blades. In figure 5 the propeller swirl is plotted and in figure 6 the pressure coefficient contours on the propeller at J = 0.8.

The error found between the CFD and the experiment is generally low except for high advance coefficient values. The error is defined as;

$$Error = \left| \frac{CFD - Experiment}{\max(CFD, Experiment)} \right|$$

Table 4. Propeller performance from CFD and experiment

	CFD			EXPERIMENT			ERROR %		
J	K_t	$10K_q$	η_0	K_t	$10K_q$	η_0	K_t	$10K_q$	η_0
0.05	0.463	0.669	0.055	0.492	0.691	0.057	5.89	3.18	3.51
0.1	0.447	0.652	0.109	0.472	0.667	0.113	5.30	2.25	3.54
0.15	0.43	0.632	0.162	0.45	0.64	0.168	4.44	1.25	3.57
0.2	0.412	0.611	0.215	0.427	0.613	0.222	3.51	0.33	3.15
0.25	0.393	0.589	0.266	0.403	0.584	0.275	2.48	0.85	3.27
0.3	0.373	0.565	0.315	0.378	0.554	0.326	1.32	1.95	3.37
0.35	0.353	0.54	0.364	0.353	0.524	0.375	0.00	2.96	2.93
0.4	0.33	0.512	0.411	0.327	0.493	0.423	0.91	3.71	2.84
0.45	0.307	0.484	0.455	0.302	0.462	0.468	1.63	4.55	2.78
0.5	0.284	0.455	0.496	0.276	0.43	0.511	2.82	5.49	2.94
0.55	0.259	0.424	0.534	0.25	0.398	0.551	3.47	6.13	3.09
0.6	0.233	0.394	0.566	0.225	0.366	0.586	3.43	7.11	3.41
0.65	0.207	0.362	0.593	0.199	0.333	0.617	3.86	8.01	3.89
0.7	0.181	0.33	0.612	0.172	0.299	0.642	4.97	9.39	4.67
0.75	0.154	0.296	0.622	0.145	0.264	0.657	5.84	10.81	5.33
0.8	0.128	0.262	0.619	0.118	0.228	0.656	7.81	12.98	5.64
0.85	0.1	0.227	0.596	0.089	0.191	0.63	11.00	15.86	5.40
0.9	0.072	0.189	0.541	0.058	0.151	0.553	19.44	20.11	2.17
0.95	0.042	0.15	0.421	0.026	0.109	0.361	38.10	27.33	14.25

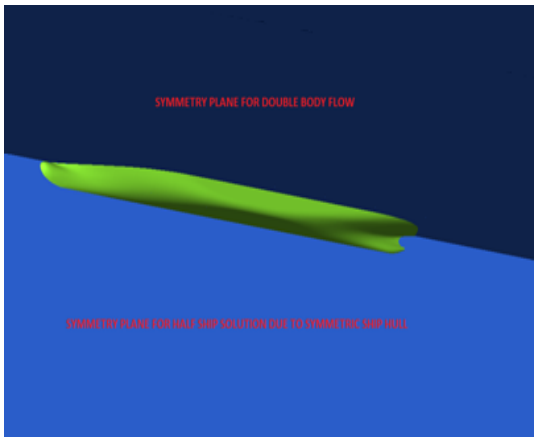

Figure 7. A perspective view of the bare hull domain.

5. CFD Validation for Bare Hull

The flow around the bare hull is solved with 1.2 million tetrahedral mesh elements. Only half of the hull is modeled in the solver due to symmetric hull form. The effects of wave resistance have been ignored therefore the analysis covers only a double body flow solution. A better view of the fluid domain has been generated in figure 7.

The water density is 998.8kg/m^3 and the water kinematic viscosity is 1.09*10^{-6}m^2/s for convenience with reference [15]. Realizable $k-\varepsilon$ turbulence model with standard wall function has been used. The effects of cavitation and free surface have been neglected. The turbulent intensity is 1% and turbulent viscosity ratio is 1. The least square cell based SIMPLE scheme for pressure-velocity coupling has been used. The pressure, momentum, turbulent kinetic energy and turbulent dissipation rate are all in second order. With default under relaxation factors, there were some problems regarding the convergence of the solution; therefore, momentum, turbulent kinetic energy and turbulent dissipation rate under relaxation factors were all set to 0.1. The number of iterations has been increased due to the choice of these factors but the results were stable. After around 10,000 iterations solutions have converged.

The total resistance coefficient of the hull can be decomposed into three components;

$$C_T = C_F + C_{VP} + C_W$$

Here; C_F is the frictional resistance coefficient, C_{VP} is the viscous pressure resistance coefficient and C_W is the wave resistance coefficient. The free surface effects are neglected therefore wave resistance equals to zero:

$$C_W = 0 \rightarrow C_T = C_F + C_{VP}$$

In this study, the total resistance can be found by adding the viscous pressure resistance and frictional resistance. The frictional resistance coefficient may be calculated from the ITTC57 correlation line which is given by the formula;

$$C_F = \frac{0.075}{(\log Re - 2)^2}$$

Re is the Reynolds number which is given as;

$$Re = \frac{v \cdot L}{\vartheta}$$

The values of frictional resistance coefficient C_F and total resistance coefficient C_T are given in table 5. The biggest error percentage is around 2.5% in C_F, while it is about 3.5% in C_T. The error is calculated as;

$$Error = \left| \frac{C_{(CFD)} - C_{(Exp)}}{\max(C_{(Exp)}, C_{(CFD)})} \right|$$

It may be said that CFD results are quite compatible with those from experiments.

Table 5. Calculated resistance coefficients from CFD and experiment

	CFD		EXPERIMENT		ERROR %	
v (m/s)	C_F x 10^3	C_T x 10^3	C_F x 10^3 (ITTC)	C_T x 10^3	C_F	C_T
1.335	3.249	3.676	3.170	3.661	2.432	0.408
1.401	3.220	3.643	3.142	3.605	2.422	1.043
1.469	3.200	3.621	3.116	3.588	2.625	0.911
1.535	3.185	3.596	3.092	3.602	2.920	0.167
1.602	3.179	3.585	3.069	3.623	3.460	1.049
1.668	3.126	3.544	3.047	3.670	2.527	3.433

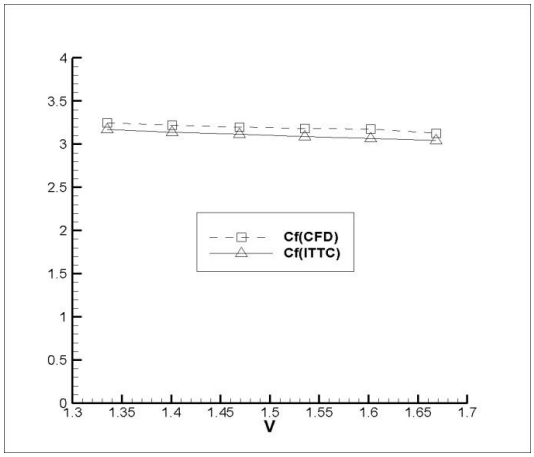

Fig. 8a. Comparison of CFD and experiment for C_F

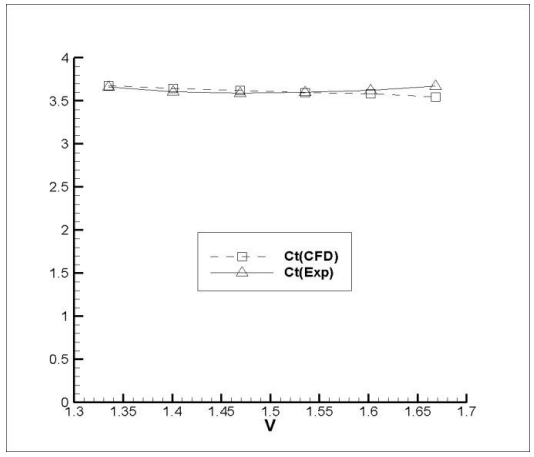

Fig. 8b. Comparison of CFD and experiment for C_T

The C_F and C_T values can also be seen in figures 8a and 8b, respectively.

The form factor has been given as 0.145 for the full scale ship in reference [15]. The form factor of the ship is found to be 0.131. This is a satisfactory result.

6. Ship – Propeller Interaction Effect on Propeller Performance

To catch the effects of the hull on the propeller and due to the highly turbulent incoming flow to the propeller behind the ship, a finer mesh of around 6 million tetrahedral elements is used. The water density and kinematic viscosity is selected to be the same as in the case of open water problem, which were 998.47kg/m^3 and 1.044*10^{-6}m^2/s, respectively. Realizable $k-\varepsilon$ turbulence model with standard wall function is used and the effects of cavitation are ignored. The propeller – ship system is deeply submerged in water; therefore, the flow is a double body solution and there are no free surface effects taken into account. The fluid domain is divided into two parts; the first involves the propeller wake which rotates with the propeller and the second is the (theoretically) unbounded fluid domain that the ship is moving in. The propeller has a rotation and thus there is no symmetry for half of a ship solution; therefore the whole underwater hull is modeled. A better view of the fluid domain is shown in figure 9.

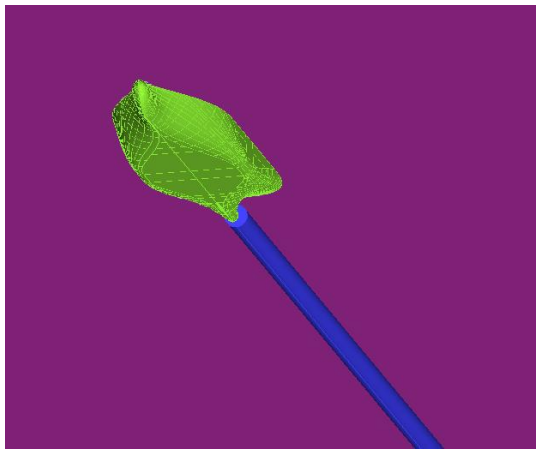

Fig. 9. A perspective view of the fluid domain from the bottom. The blue cylinder contains the propeller and represents the wake.

The inlet velocity is held constant in the analyses and the number of revolutions of the propeller is constantly changed to have a new advance coefficient J. The domain representing the propeller wake moves along with the propeller.

The turbulent intensity is 1% and turbulent viscosity ratio is 1. The least square cell based SIMPLE scheme for pressure-velocity coupling is used. The pressure, momentum, turbulent kinetic energy and turbulent dissipation rate are all in second order. The convergence of the solution is satisfied and the relaxation factors are decreased if needed. After around 10,000 iterations, solutions are found to have converged.

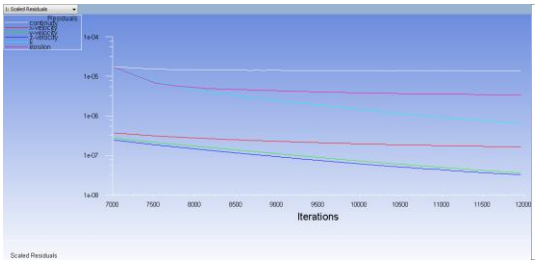

Fig. 10. Residuals in logarithmic scale show the convergence of the solution.

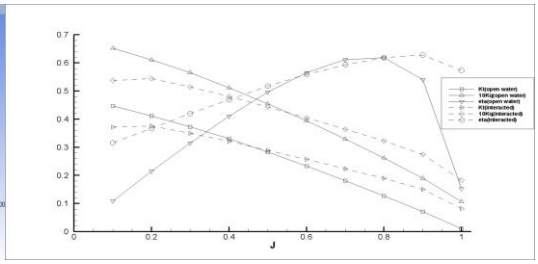

Fig. 11. Effect of ship hull on propeller performance

Figure 10 shows the convergence of the solution for the advance coefficient J = 0.6.

The ship causes a change in the incoming velocity to the propeller plane and the velocity differs at each part of the disc. The velocity that the propeller is working in the interacted case is calculated by dividing the surface integral for velocity by the area of the propeller disc. This operation gives only one area weighted average velocity for the propeller. The advance coefficient in the interacted case uses this area weighted average velocity.

The effects of the ship on propeller performance (K_t, K_q, η_0) can be seen in figure 11.

A tabulated form of figure 11 is given in table 6. The interaction of propeller with the ship hull changes the performance of the propeller greatly.

In the case of ship hull, the thrust coefficient of the propeller decreases in low advance coefficients and increases in high advance coefficients with respect to the case of no ship hull (open water case). However, this variation in thrust is compensated by the variation in the torque coefficient. In most cases, (except small efficiency losses in advance coefficients between 0.6 and 0.8), the propeller efficiency is higher in the interacted case than the one in open – water case. The maximum efficiency in open – water was 0.6188 at J = 0.8, while in the interacted case it is 0.6278 at J = 0.9.

The path-lines exerted from the blades of the propeller are more chaotic when compared to the open – water case. The propeller swirl for J = 0.661 of the interacted case is shown in figure 12a. The wake of propeller is contracted much more in the case of ship-propeller interaction than in the case of open-water. It is possible that the flow is affected by the turbulence produced behind the ship and that the propeller wake shows better performance in open water. The propeller swirl for J = 0.661 for the open water case is given in figure 12b.

Table 6. Effect of ship hull on propeller performance

	OPEN – WATER CASE			HULL-INTERACTED CASE		
J	K_t	$10K_q$	η_0	K_t	$10K_q$	η_0
0.1	0.4468	0.6517	0.1091	0.3721	0.5372	0.3157
0.2	0.4118	0.6110	0.2145	0.3754	0.5441	0.3671
0.3	0.3733	0.5653	0.3153	0.3494	0.5141	0.4201
0.4	0.3302	0.5119	0.4106	0.3215	0.4811	0.4689
0.5	0.2836	0.4547	0.4963	0.2894	0.4431	0.5176
0.6	0.2333	0.3937	0.5659	0.2572	0.4046	0.5588
0.7	0.1810	0.3295	0.6120	0.2235	0.3639	0.5935
0.8	0.1275	0.2623	0.6188	0.1898	0.3226	0.6181
0.9	0.0715	0.1894	0.5405	0.1501	0.2743	0.6278
1	0.0103	0.1069	0.1534	0.0817	0.1836	0.5729

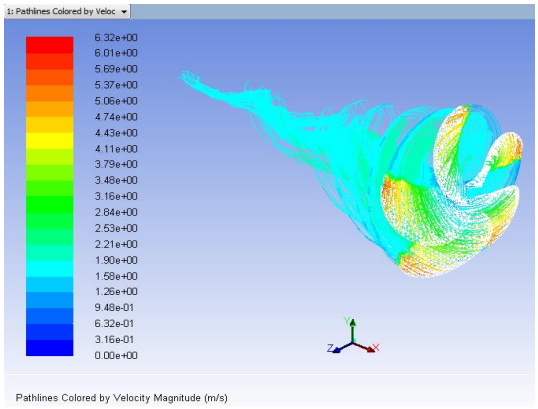

Fig. 12a. Propeller swirl in the case with the ship hull.

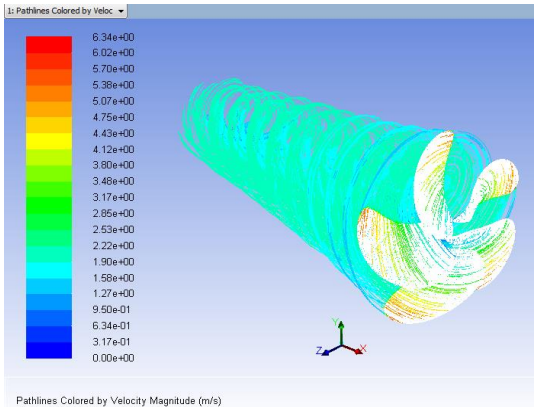

Fig. 12b. Propeller swirl in open water

The pressure coefficients at the aft part of the ship including the propeller are given in figure 13 which shows the contours for the face and the back sides of the propeller. The effective wake (no rudder effect is considered in this study) can be seen in figure 14a along with the nominal wake shown in figure 14b. The effective and nominal wake contours are taken from the propeller axis. Figures are given for J = 0.661.

The results produced from CFD analyses must be compared with those of experimental propulsion tests for validation. To do this, the self-propulsion point of the model should be determined. The velocity of the model is set to be 1.335m/s and by using table 4, total resistance coefficient can be found to be $C_T = 3.661 \cdot 10^{-3}$ by interpolation technique. The total resistance is then;

$$R_T = \frac{1}{2}\rho S_w v^2 C_T$$

$$= \frac{1}{2} \cdot 998.47 \cdot 6.243 \cdot 1.335^2 \cdot 3.661 \cdot 10^{-3} \cong 20.34N$$

The propeller should generate a thrust force to overcome this total resistance plus the extra resistance by itself from the thrust deduction factor..

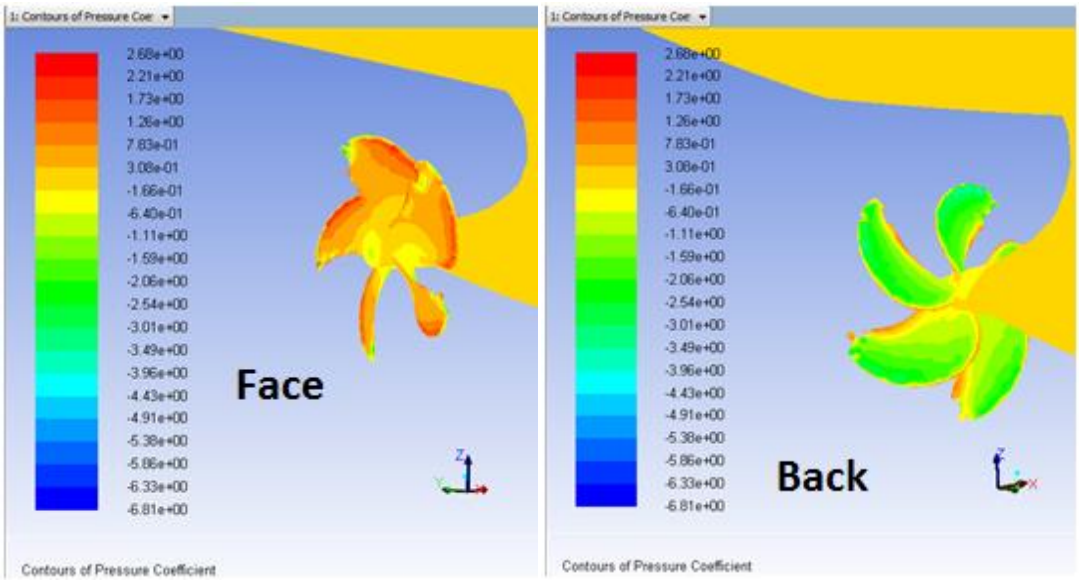

Figure 13. Contours of pressure coefficient at the aft

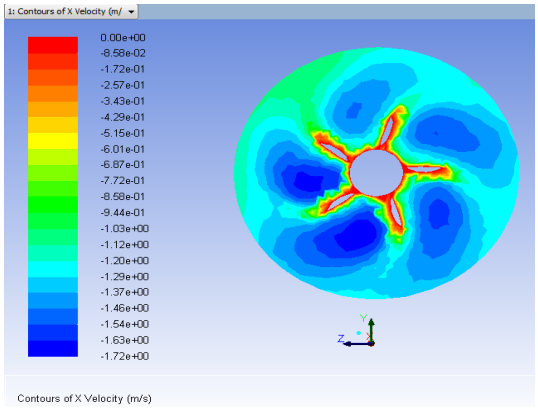

Fig. 14a. Effective wake

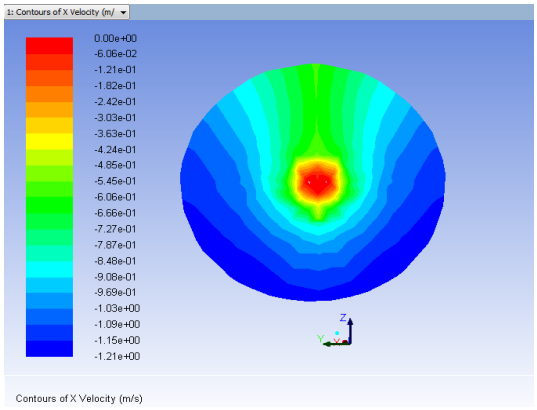

Fig. 14b. Nominal wake

However, a quick estimation made with the resistance of the bare hull will lead to a total resistance being equal to the thrust. From table 3 for the interacted case and by using the thrust coefficient equation; it can be found that K_t for self-propulsion point must lie between J = 0.6 and J = 0.7:

$$J = 0.6 \rightarrow K_t = 0.2333 \rightarrow T_{J=0.6} \cong 28.61N$$
$$J = 0.7 \rightarrow K_t = 0.7 \rightarrow T_{J=0.7} \cong 18.26N$$

Total resistance of the bare hull corresponds to a point between these values. However, a point that is satisfied for $T - R_T = 0$, must be found

This value must be obtained for the best value of the self-propulsion advance coefficient. An initial guess for an advance coefficient should be made and at the last guess $T - R_T = 0$ must be supplied. The estimation for the self-propulsion advance coefficient is found as 0.661. The difference between the thrust and the total resistance is found to be -0.2 for this advance coefficient which is sufficient for the current case.

After the analysis converged for J = 0.661, the thrust and torque values are read from the solver. Thrust and torque coefficients for the interacted case is found to be;

$K_{t(interacted)} = 0.237$, $K_{q(interacted)} = 0.038$

Then these values are found for the interacted case and the open – water propeller test is applied to the propeller for the self-propulsion advance coefficient. The thrust and torque coefficients for the open – water propeller case is found as;

$K_{t(open-water)} = 0.202$, $K_{q(open-water)} = 0.036$

The relative rotative efficiency is given as;

$$\eta_R = \frac{K_{q(open-water)}}{K_{q(interacted)}}$$

The relative rotative efficiency is calculated for the self-propulsion point as;

$$\eta_R = 0.947$$

This value is found to be 0.959 in the experiment. The error percentage when compared to the experiment is found to be around 1%.

The hull efficiency is given as;

$$\eta_H = \frac{1-t}{1-w}$$

The hull efficiency depends on thrust deduction factor and wake coefficient. These coefficients are defined as;

$$t = 1 - \frac{R_T}{T}$$
$$w = 1 - \frac{v_A}{V}$$

Here; T is the thrust supplied by the propeller to the ship hull while R_T is the total resistance of the ship hull without the propeller. v_A is calculated by surface integration of the axial velocities and dividing them by the propeller disc area. v is the ship speed.

Following this notation, the thrust deduction factor and wake coefficient are found to be;

$$t = 1 - \frac{20.34}{21.71} = 0.063 \quad and \quad w = 1 - \frac{1.182}{1.335} = 0.115$$

Therefore; the hull efficiency becomes,

$$\eta_H = \frac{1-0.063}{1-0.115} = 1.059$$

The hull efficiency has been found to be $\eta_H = 1.249$ in reference [15]. However in the original paper [15], self – propulsion point is calculated by interpolation over measurement

results while in this study the self – propulsion point is found with an iterative manner. The thrust gradients over advance coefficients may be high and therefore, calculation of self – propulsion point with interpolation may guide to different results. It can be said that the hull efficiency found with this way is more reliable.

7. Conclusion

The hull effect on the propeller performance of the Duisburg Test Case hull has been examined in this paper. First, the propeller in the open – water and the bare hull has been solved and the results have been compared with those of experiments for the validation and calibration of CFD solver. After satisfactory results have been obtained for both cases, the ship with a rotating propeller has been solved in the solver to investigate the hull effect on the propeller. Even though the efficiency in the open – water case of the propeller has big curvature, it is in the interacted case found to be much flatter. Changes in the advance coefficients affect the hull – interacted case lesser. Maximum efficiency in the interacted case is found to be higher than the open – water case. Maximum efficiency in the open water case is at J = 0.8 while it is J = 0.9 for the hull – interacted case. The results were justified by calculating the relative rotative and hull efficiencies of the propeller – hull system.

In terms of propulsion performance of the Duisburg Test Case Hull, the rudder also plays an important role. The solution in this study is given without the effects of rudder on the propeller performance. An actual case should include the rudder with the possible effects of cavitation and free water surface.

The reference article [15] does not state whether the propeller is optimized or not. Propeller optimization will increase the propulsion efficiency of the ship. An integrated work covering all the aspects of the real case will provide with better results for a propeller optimization which will lead us to take one more step ahead for a better initial design.

Acknowledgements

This study is funded by Istanbul Technical University Scientific Research Coordinatorship.

References

[1] Zhang, Z., Liu, H., Zhu, S., Zhao, F., *Application of CFD in ship engineering design practice and ship hydrodynamics*, Journal of Hydrodynamics, Vol. 18, Issue 3, July 2006, p. 315 – 322

[2] Zhou, L. D., Yuan, J. L., *Calculation of the turbulent flow around the stern and in the wake of a body of revolution with the propeller in operation*, 15th Symposium on Naval Hydrodynamics, 1984, p. 279 – 290

[3] Shen, H., Gomri, A., Chen, Q., *The hydrodynamic performance prediction of ship hull with propeller*, International Conference on Applied Mechanics, Materials and Manufacturing, 2011, Vol. 117 – 119, p. 598 – 601, Shenzhen

[4] Tocu, A. M., Lungu, A., *Free – surface flow features in the stern region of a propelled ship*, Numerical Analysis and Applied Mathematics International Conference, 2008, p. 767 - 770

[5] Stück, A., Kröger, J., Rung, T., *Adjoint-based Hull Design for Wake Optimisation, Ship Technology Research, Vol. 58, Issue 1*, 2011, p. 34 – 44

[6] Lee, S. K., Chen, H. C., *The influence of propeller/hull interaction on propeller induced cavitating pressure*, ISOPE 2005, 19 – 24 June 2005, Seoul, p. 25 – 33

[7] Szelangiewicz, T., Abramowski, T., *Numerical analysis of influence of ship hull form modification on ship resistance and propulsion characteristics. Part I, influence of hull form modification on ship resistance characteristics*, Polish Maritime Research, 2009, 4, 62, Vol. 16, p. 3 – 8

[8] Szelangiewicz, T., Abramowski, T., *Numerical analysis of influence of ship hull form modification on ship resistance and propulsion characteristics. Part II, influence of hull form modification on wake current behind the ship*, Polish Maritime Research, 2010, 4, 63, Vol. 17, p. 3 – 9

[9] Szelangiewicz, T., Abramowski, T., *Numerical analysis of influence of ship hull form modification on ship resistance and propulsion characteristics. Part III, influence of hull form modification on screw propeller efficiency*,

Polish Maritime Research, 2010, 4, 63, Vol. 17, p. 10 – 13

[10] Lungu, A., Pacuraru, F., *Numerical study of the hull-propeller-rudder interaction*, Numerical Analysis and Applied Mathematics, International Conference 2009, Vol. 2, p. 693 – 696

[11] Muscari, R., Felli, M., Di Mascio, A., *Analysis of the flow past a fully appended hull with propellers by computational end experimental fluid dynamics*, Journal of Fluids Engineering, Vol. 133, 2011

[12] Felli, M., Di Felice F., *Propeller wake analysis in nonuniform inflow by LDV phase*, Journal of Marine Science and Technology, 2005, p. 159 – 172

[13] Felli, M., Roberto, C., Guj, G., *Experimental analysis of the flow around a propeller-rudder configuration*, Experiments in Fluids, 2009, p. 147 – 164

[14] Carlton, J., Radosavljevic, D., Whitworth, S., *Rudder – Propeller – Hull Interaction: The Results of Some Recent Research, In-Service Problems and Their Solutions*, First International Symposium on Marine Propulsors, June 2009, Trondheim

[15] el Moctar, O., Shigunov, V., Zorn, T., *Duisburg Test Case: Post-Panamax Container Ship for Benchmarking*, Ship Technology Research, August 2012, Vol. 59, No. 3, p. 50 – 65

[16] Versteeg, H. K., Malalasekera, W., *An Introduction to Computational Fluid Dynamics, The Finite Volume Method*, 1st ed., 1995

[17] Brandner, P., *Calculation results for the 22nd ITTC Propulsor Committee Workshop on Propeller RANS/PANEL Methods*, 22nd ITTC Propulsion Committee Propeller RANS/Panel Method Workshop, 5 – 6 April 1998, Grenoble

[18] Bal, S., *A method for optimum cavitating ship propellers*, Turkish J. Eng. Env. Sci., 2011, 35, p. 139 – 158